VeCoR — **Velocity Contrastive Regularization for Flow Matching**

Zong-Wei Hong Jing-lun Li Lin-Ze Li Shen Zhang Yao Tang JIIOV Technology

{zongwei.hong, jinglun.li, linze.li, shen.zhang, yao.tang}@jiiov.com

Abstract

Flow Matching (FM) has recently emerged as a principled and efficient alternative to diffusion models. Standard FM encourages the learned velocity field to follow a target direction; however, it may accumulate errors along the trajectory and drive samples off the data manifold, leading to perceptual degradation, especially in lightweight or lowstep configurations.

To enhance stability and generalization, we extend FM into a balanced attract—repel scheme that provides explicit guidance on both "where to go" and "where not to go." To be formal, we propose Velocity Contrastive Regularization (VeCoR), a complementary training scheme for flow-based generative modeling that augments the standard FM objective with contrastive, two-sided supervision. VeCoR not only aligns the predicted velocity with a stable reference direction (positive supervision) but also pushes it away from inconsistent, off-manifold directions (negative supervision). This contrastive formulation transforms FM from a purely attractive, one-sided objective into a two-sided training signal, regularizing trajectory evolution and improving perceptual fidelity across datasets and backbones.

On ImageNet-1K 256×256, VeCoR yields 22% and 35% relative FID reductions on SiT-XL/2 and REPA-SiT-XL/2 backbones, respectively, and achieves further FID gains (32% relative) on MS-COCO text-to-image generation, demonstrating consistent improvements in stability, convergence, and image quality, particularly in low-step and lightweight settings.

1. Introduction

Flow Matching (FM) [24, 25] learns a time-dependent velocity field that transports probability mass along a prescribed path between a reference distribution and the data. This viewpoint makes precise connections to diffusion/score-based modeling via the probability-flow formulation [19, 40], to continuous normalizing flows [7, 14], and to optimal transport through dynamical formulations [5, 32]. FM and its rectified variants have demonstrated competitive performance in image synthesis [24, 25].

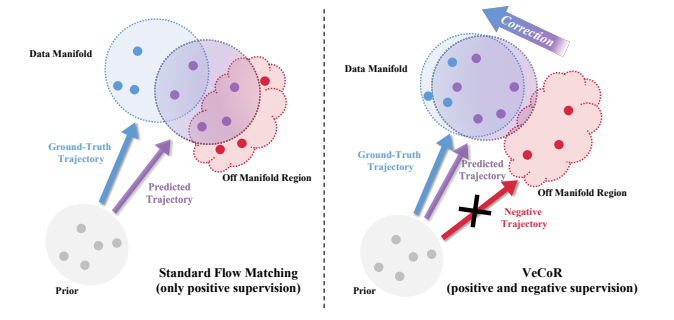


Figure 1. Supervision and trajectory behavior. Left—Standard Flow Matching (SFM): trained only with positive supervision toward the ground-truth velocity (blue), the predicted trajectory (purple) may slightly deviate from the data manifold, sometimes leading to less stable generations. Right—VeCoR: by contrastively suppressing negative trajectories (red path and ×), VeCoR adds negative supervision that discourages off-manifold deviations and guides trajectories back toward the data manifold, improving stability and perceptual fidelity.

While FM provides a theoretically elegant and empirically powerful foundation, subtle challenges can still arise in practice, particularly under lightweight or low-step configurations. In such settings, the integration process may accumulate minor inconsistencies in the learned velocity field, causing samples to drift slightly away from the data manifold, as illustrated in Fig. 1 (left). This drift often manifests as mild perceptual degradations, such as desaturated colors, geometric misalignment, or blurred boundaries (see qualitative examples in Fig. 2). These observations suggest that, although FM effectively directs samples toward the data manifold, it may benefit from complementary regularization that further stabilizes trajectory evolution and helps maintain perceptual consistency.

Building on extensive efforts to simplify and stabilize the transport process, including methods that enforce straighter ODE trajectories, reduce function evaluations, or leverage distillation techniques [22, 36, 38, 45], we revisit the supervision dynamics of Flow Matching from a complementary perspective. We move beyond a sole focus on the accuracy of predicted velocities and broaden the notion of supervision to encompass both attractive and repulsive guidance,

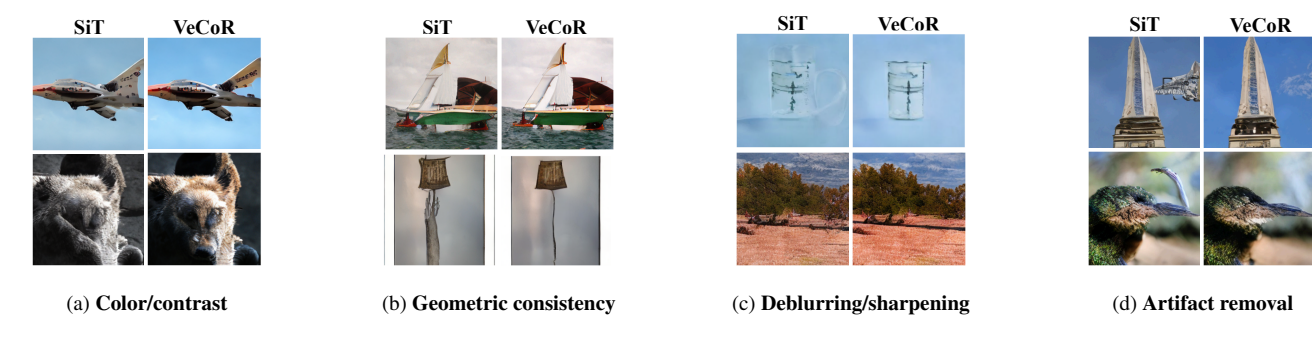


Figure 2. VeCoR refines strong SiT baselines by suppressing negative trajectories and improving stability and perceptual fidelity. Although SiT already produces plausible ImageNet-1K 256×256 samples, its sampling trajectories can still drift from the ground truth, causing color/contrast shifts, geometric distortions, blur, and artifacts; VeCoR reduces these issues under identical sampling (same seed, 50 NFEs, Euler–Maruyama). (a) Color/contrast: VeCoR yields a more saturated, uniform sky and wolf hues closer to the ground truth. (b) Geometric consistency: SiT bends the boat and distorts the lamp shade, while VeCoR produces a level hull and a lamp shade closer to the true shape. (c) Deblurring/sharpening: previously soft boundaries become crisp. (d) Artifact removal: SiT hallucinates extraneous structures (e.g., a mechanical arm near the spire; a protrusion above the bird's beak), whereas VeCoR removes them, restoring clean, plausible shapes and textures.

yielding a more balanced treatment of trajectory learning. This perspective hypothesizes that incorporating a gentle repulsive component can further harmonize the learning dynamics, encouraging models not only to follow reliable flow directions but also to maintain stability and coherence along the manifold.

Building on the strong foundation of Flow Matching, we introduce Velocity-Contrastive Regularization (VeCoR), a complementary training scheme designed to enhance the stability and robustness of learned velocity fields. VeCoR extends the conventional objective by jointly encouraging attraction toward ground-truth velocities and contrastive repulsion from dynamics-inconsistent counterparts. Rather than altering the core formulation of Flow Matching, VeCoR enriches it with supervision that goes beyond simple pointwise alignment by introducing negative velocity samples—plausible yet gently perturbed directions that provide explicit contrastive cues for more balanced, two-sided guidance. These negatives are synthesized through semanticpreserving, augmentation-like perturbations applied across image, latent, and velocity domains, ensuring scalability, generality, and seamless integration into existing frameworks. This attract–repel formulation regularizes trajectory dynamics by suppressing drift along off-manifold directions and promoting correction toward the data manifold, as illustrated in the right panel of Fig. 1

We empirically evaluate VeCoR across multiple image generation benchmarks and observe that it achieves higher sample quality and noticeably faster convergence than standard Flow Matching setups, while also improving training stability and generalization. The main contributions of this work are summarized as follows:

 We propose a complementary training scheme for flowbased generative models that augments standard super-

- vision with an ensemble of stable and perturbed flows, improving sample quality and convergence without extra data or architectural changes.
- We introduce Velocity Contrastive Regularization (VeCoR), a contrastive loss on the velocity field that enforces directional consistency of generative trajectories, yielding more stable and faster training.
- Empirically, VeCoR delivers strong gains: on ImageNet-1K, it yields 22% and 35% relative FID reductions on SiT-XL/2 and REPA-SiT-XL/2 backbones, respectively, and a further 32% FID reduction on MS-COCO text-toimage generation, indicating consistent improvements in stability, convergence, and image quality, especially in low-step and lightweight settings.

2. Related Work

Recent advances in generative modeling have been shaped by two dominant paradigms: diffusion-based models [18, 39, 40] and flow-matching (FM) approaches [24, 25]. Diffusion models formulate data generation as a stochastic denoising process that gradually perturbs data with noise and learns to reverse this process through score or noise prediction. Extensive research has improved their stability and sampling efficiency through enhanced ODE/SDE solvers [26, 27, 39, 44] and step-reduction or distillation techniques [12, 29, 36, 45].

Flow Matching (FM), by contrast, learns a continuous velocity field that deterministically transports a simple prior toward the data manifold [24, 25]. It offers a unified perspective connecting diffusion models, optimal transport [13, 32], and continuous normalizing flows [6, 14], achieving diffusion-level generative quality with far fewer integration steps. FM thus combines theoretical clarity

with computational efficiency, motivating a growing body of work exploring its dynamics and extensions.

Building on these foundations, Stochastic Interpolants [2, 25] further unify score-driven and velocity-driven formulations within a shared drift-diffusion structure, providing geometric insight into generative dynamics. Subsequent studies have sought to simplify or regularize the learned transport map by straightening trajectories, adopting adaptive integration schemes, or employing rectified formulations, thereby yielding smoother and more stable flows [22, 38]. Together, these developments have progressively refined how continuous flows are represented and optimized.

While recent progress has significantly enhanced efficiency and smoothness, most objectives in FM remain directionally one-sided: they attract the model toward correct velocities but provide limited feedback on how to actively repel unstable or inconsistent dynamics. This suggests an opportunity for complementary training signals that jointly shape attractive and repulsive components of the flow.

A concurrent effort, Contrastive Flow Matching (Δ FM) [41], augments the FM objective with contrastive signals to improve conditional generation. By separating flows across distinct conditions, Δ FM enhances class discriminability and mitigates ambiguity. Our approach, in contrast, applies contrastive regularization at the level of dynamics stability rather than conditional separation—serving as a general stabilization mechanism that complements existing FM objectives and preserves structural coherence throughout trajectory evolution.

3. Preliminaries

Building upon the problem formulation discussed in the introduction, this section formalizes the flow-matching process and establishes the mathematical groundwork that motivates our later velocity contrastive regularization.

Problem Setup. Given two arbitrary probability distributions, a prior p_0 and a target p_1 , the objective of flow matching is to learn a vector field that transports samples from the former to the latter. In the context of generative modeling, p_0 is typically chosen as a simple distribution, such as a standard Gaussian $\mathcal{N}(0,I)$, while p_1 represents the true data distribution p(x). Following the framework of Stable Diffusion [35], we model the image distribution p(x) in the latent space rather than pixel space. Specifically, each image \hat{I} is first encoded into a latent representation \hat{x} using a pretrained variational autoencoder encoder, upon which the flow field is learned to approximate the generative process.

Stochastic Interpolants. For any given sample $\epsilon \sim \mathcal{N}(0,I)$ and data point $\hat{x} \sim p(x)$, flow matching progressively transforms noise into data over a continuous time interval. This transformation can be formalized as a time-dependent stochastic process using stochastic inter-

polants [2, 28], defined by

$$\hat{x}_t = \alpha_t \hat{x} + \sigma_t \epsilon, \tag{1}$$

where α_t and σ_t denote time-dependent scheduling functions for $t \in [0,1]$, subject to the boundary conditions $\alpha_1 = \sigma_0 = 1$ and $\alpha_0 = \sigma_1 = 0$. Although non-linear parameterizations of α_t and σ_t are possible, linear schedules are generally sufficient to achieve strong performance in diffusion models. Therefore, in our experiments, we simply set $\alpha_t = t$ and $\sigma_t = 1 - t$.

Learning Objective. The path induced by the interpolant in Eq. (1) corresponds to the solution of a probability flow ordinary differential equation [28, 40], governed by a time-dependent velocity field $\hat{\mathbf{v}}(\hat{x},t,\epsilon)$. The model learns a neural network $\mathbf{v}_{\theta}(\hat{x}_t,t)$ that approximates this field. The ground-truth target velocity for the interpolated path is

$$\hat{\mathbf{v}}(\hat{x}, t, \epsilon) = \dot{\alpha}_t \hat{x} + \dot{\sigma}_t \epsilon, \tag{2}$$

where $\dot{\alpha}_t$ and $\dot{\sigma}_t$ are time derivatives of the scheduling functions.

The standard flow-matching objective minimizes the mean-squared error (MSE) to this target:

$$\mathcal{L}^{(\mathrm{FM})}(\boldsymbol{\theta}) = \mathbb{E}_{t,\hat{x},\epsilon} [\|\mathbf{v}_{\boldsymbol{\theta}}(\hat{x}_t,t) - \hat{\mathbf{v}}(\hat{x},t,\epsilon)\|^2]. \quad (3)$$

With a finite training dataset $S_{train} = \{(\hat{x}^{(i)}, t^{(i)}, \epsilon^{(i)})\}_{i=1}^N$, this objective is implemented empirically as

$$\widehat{\mathcal{L}}^{(\text{FM})}(\boldsymbol{\theta}; \mathcal{S}_{train}) = \frac{1}{N} \sum_{i=1}^{N} \left\| \mathbf{v}_{\boldsymbol{\theta}}(\hat{x}_{t^{(i)}}^{(i)}, t^{(i)}) - \hat{\mathbf{v}}(\hat{x}^{(i)}, t^{(i)}, \epsilon^{(i)}) \right\|^{2}.$$
(4)

Toward Better Regularization. While the empirical objective in Eq. (4) has proven highly effective for learning the overall transport dynamics, it primarily supervises where trajectories should move, offering limited guidance on where they should not. Under constrained data or model capacity, this directional asymmetry may leave certain regions of the learned flow insufficiently regularized, allowing local instabilities to emerge. These observations suggest an opportunity to enrich FM training with complementary signals that provide balanced guidance—not only encouraging accurate motion toward the data manifold, but also discouraging inconsistent or dynamically unstable directions within the velocity space.

4. Method

This section introduces **Velocity-Contrastive Regularization (VeCoR)**, a training scheme that augments standard Flow Matching with explicit negative guidance at the level of the velocity field. Our key insight is to treat the learned

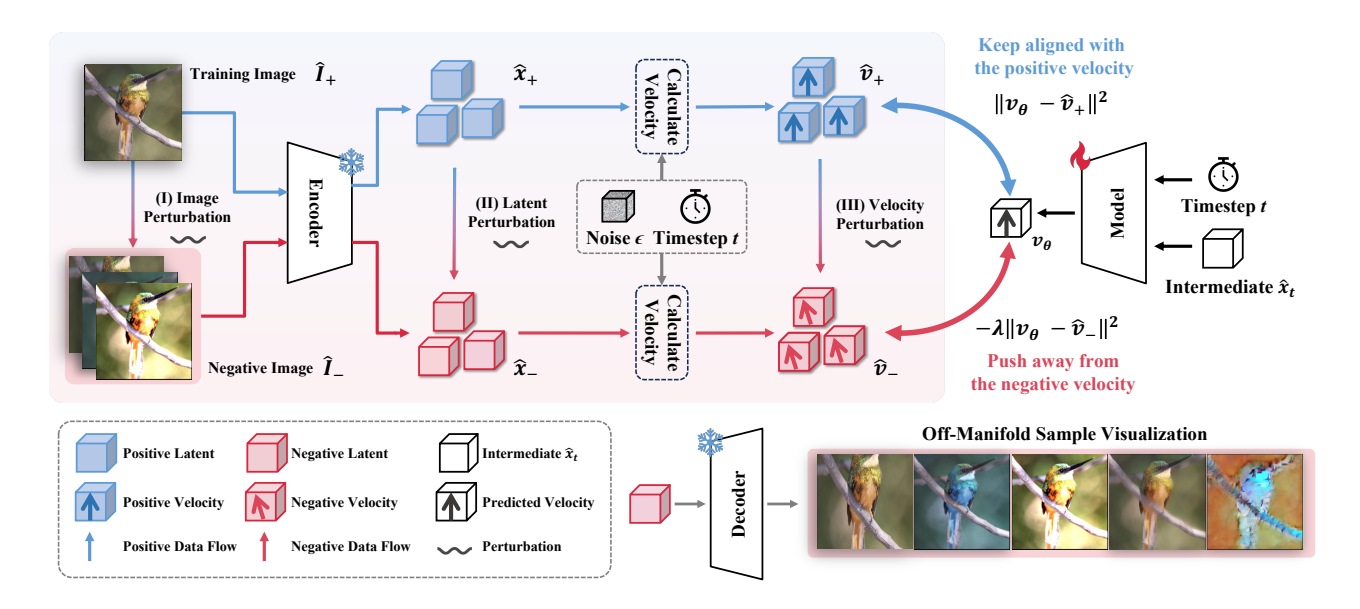


Figure 3. Overview of the proposed Velocity-Contrastive Regularization (VeCoR) framework. VeCoR enhances flow matching (FM) by introducing a balanced, bidirectional supervision mechanism in the velocity space. Instead of relying solely on positive guidance toward the ground-truth flow, VeCoR incorporates complementary contrastive cues that define counter-directional references across multiple representational domains. These perturbations—spanning (I) image, (II) latent, and (III) velocity spaces—are implemented through lightweight, augmentation-like transformations that preserve semantic consistency while altering dynamic behaviors. The resulting positive and negative velocities, \hat{v}_+ and \hat{v}_- , jointly guide the model-predicted velocity v_θ toward stable and coherent dynamics while discouraging drifts toward unstable regions. The visualization (bottom right) illustrates how negative velocity guidance can induce off-manifold deviations, leading to degraded sample quality.

velocity itself as editable data and to synthesize *local negative velocity candidates* via augmentation-like perturbations in image, latent, or velocity space. These negatives are semantically consistent but dynamically perturbed, and are used to repel the model away from unstable or off-manifold directions, while the standard FM loss continues to attract it toward the ground-truth flow.

We formalize the VeCoR objective in Sec. 4.1 and describe negative velocity candidates in Sec. 4.2.

4.1. Velocity-Contrastive Regularization

To enrich the supervision of flow matching, we introduce a contrastive regularization term that provides *negative guidance*. Instead of solely aligning predicted and target velocities, VeCoR expands training into a two-sided process that attracts the model toward reliable flow directions while gently repelling it from unstable or off-manifold ones. This contrastive formulation complements the empirical FM objective by regularizing regions of the state space that remain underconstrained under finite data and model capacity, thereby improving flow stability and generative fidelity.

We view the predicted velocity field as editable data, from which informative negative samples can be synthesized. Concretely, we expand the finite training set by introducing semantically consistent yet dynamically perturbed velocity directions drawn from a pool of negative candidates (see Sec. 4.2). This augmentation-like perturbation scheme transforms each supervised instance into a set of semantically consistent yet statistically perturbed alternatives: one positive and several repulsive negatives, encouraging the model to refine its generative flow through explicit contrastive regularization.

Formally, for each velocity $\hat{\mathbf{v}}_{+}^{(i)} \coloneqq \hat{\mathbf{v}}(\hat{x}^{(i)}, t^{(i)}, \epsilon^{(i)}) \in \mathcal{S}_{\text{train}}$, we construct a finite set of candidate velocities:

$$C_i = \{\hat{\mathbf{v}}_-^{(i1)}, \dots, \hat{\mathbf{v}}_-^{(iK)}\}, \tag{5}$$

where the negatives $\{\hat{\mathbf{v}}_{-}^{(ij)}\}_{j=1}^{K}$ are selected to be plausible yet misleading velocity directions. We then augment the training data via

$$\widetilde{\mathcal{S}}_{\text{train}} = \mathcal{S}_{\text{train}} \ \cup \ \bigcup_{i=1}^{N} \mathcal{C}_{i}.$$
 (6)

Given this augmented setup, learning proceeds by aligning with the positive and repelling from the negatives. We regularize the model by pushing its predicted velocity away from the negative candidates while keeping it aligned with the true direction:

$$\widehat{\mathcal{L}}^{(\text{VeCoR})}(\boldsymbol{\theta}; \widetilde{\mathcal{S}}_{\text{train}}) = \frac{1}{N} \sum_{i=1}^{N} \left[\left\| \mathbf{v}_{\boldsymbol{\theta}}(\hat{x}_{t^{(i)}}^{(i)}, t^{(i)}) - \hat{\mathbf{v}}_{+}^{(i)} \right\|_{2}^{2} - \lambda \sum_{j=1}^{K} \left\| \mathbf{v}_{\boldsymbol{\theta}}(\hat{x}_{t^{(i)}}^{(i)}, t^{(i)}) - \hat{\mathbf{v}}_{-}^{(ij)} \right\|_{2}^{2} \right].$$
(7)

Here, $\lambda \in (0,1)$ controls the strength of the contrastive repulsion.

4.2. Negative Velocity Candidate Set

Training FM with VeCoR requires plausible but incorrect velocity samples—those that appear semantically valid yet violate the underlying flow dynamics. Instead of mining such samples from real-world data (which is costly and ill-defined), we leverage we leverage augmentation-like perturbations as a controllable and systematic perturbation mechanism. In the spirit of data augmentation commonly used in both supervised and unsupervised representation learning [3, 15, 20], these perturbations naturally expose model fragilities while preserving semantic consistency. This makes it suitable for constructing a scalable and diverse pool of negative velocity samples, consistent with the failure examples shown earlier in Fig. 2.

Our perturbation pipeline follows the taxonomy introduced by SimCLR [8], which broadly categorizes transformations into two types. The first comprises spatial or geometric transformations, such as random cropping and resizing, channel shuffling, and CutMix [43]. The second includes appearance transformations, such as color jittering, Gaussian blur, and additive Gaussian noise. Together, these complementary operations introduce controlled variations in both structure and appearance while preserving the underlying semantics of the data.

While conventional augmentation operates solely in the image space, we reinterpret these operations as augmentation-like perturbations and extend them to representational domains: image, latent, and velocity. Perturbations in each domain act at a distinct level of abstraction and are used to construct negative velocities that provide contrastive supervision, offering complementary perspectives on model robustness and feature alignment.

As illustrated in Fig. 3, the process begins with a training image \hat{I}_+ and its perturbed counterpart \hat{I}_- , generated by image-level augmentation. Passing them through the encoder yields latent representations \hat{x}_+ and \hat{x}_- . Alternatively, latent-level augmentation can be directly applied to \hat{x}_+ to obtain a perturbed latent \hat{x}_- . For simplicity, we use the unified notation \hat{x}_- for both cases, as they serve the same role in constructing negative supervision.

Given a sampled noise ϵ and timestep t, we compute the corresponding positive and negative velocities, \hat{v}_+ and \hat{v}_- ,

from \hat{x}_+ and \hat{x}_- , respectively. Additionally, velocity-level augmentation can be applied directly to \hat{v}_+ to produce a perturbed velocity \hat{v}_- . Although \hat{v}_- obtained from the encoder and \hat{v}_- obtained through direct augmentation stem from different mechanisms, both represent semantically plausible yet dynamically inconsistent flows. Hence, we collectively denote them as \hat{v}_- for unified contrastive supervision.

This design establishes a flexible and extensible framework for constructing negative candidate velocities across multiple representational domains. While our current implementation primarily demonstrates augmentation-based perturbations, the framework itself is not limited to this setting. In essence, it provides a general mechanism for generating and contrasting representations, enabling broader applications such as domain adaptation, consistency regularization, or adversarial robustness. During training, the model's predicted velocity $v_{\theta}(x_t, t)$ is encouraged to align with the positive velocity \hat{v}_+ while being repelled from the negative velocity \hat{v}_{-} , thereby enforcing bidirectional contrastive regularization within this unified framework. For completeness, the full set of augmentation-like perturbations and implementation details are provided in the supplementary material.

5. Experiments

This section first introduces the experimental setup and then presents the corresponding results.

5.1. Experimental Settings

Datasets and Implementation. We evaluate both class-conditional and text-to-image (T2I) generation tasks. For class-conditional generation, experiments are conducted on ImageNet-1k [9] at 256×256 resolution, following the preprocessing of ADM [10]. Each image is encoded using the Stable Diffusion VAE [34] into a latent tensor $\mathbf{z} \in \mathbb{R}^{32 \times 32 \times 4}$. We train vanilla SiT [1] models of various scales (S/2, B/2, L/2, XL/2) under identical hyperparameters, except for the application of our VeCoR module.

To further evaluate the generalizability of our method, we integrate REPresentation Alignment (REPA) [42] with VeCoR and train REPA models (B/2, XL/2) on ImageNet-1k at 256×256 resolution. REPA accelerates training and enhances the generative quality of conventional diffusion models by aligning their intermediate representations with pretrained vision encoders (e.g., DiNOv2 [31]) through an auxiliary distillation loss.

For T2I generation, we follow the setup of U-ViT [4, 42] and train REPA-MMDiT [11] from scratch on the MS-COCO dataset [23]. The model is trained for 150K iterations with a batch size of 256, a hidden dimension of 768, and a depth of 24. Text embeddings are derived from the CLIP [33] text encoder.

Table 1. Main results on ImageNet-1K 256×256 using SiT backbones (same seed, 50 NFEs, Euler–Maruyama), demonstrating the effectiveness of our method, VeCoR, across multiple model scales. "—" indicates results that do not exist in their paper.

Model	FID ↓	IS↑	sFID ↓	Prec. ↑	Rec. ↑
SiT-S/2 [28]	64.26	22.78	15.60	0.39	0.56
$+\Delta$ FM [41]	_	_	_	_	-
+VeCoR (Ours)	55.13	25.48	7.41	0.42	0.59
SiT-B/2 [28]	42.28	38.04	11.35	0.50	0.62
$+\Delta$ FM [41]	33.39	43.44	5.67	0.53	0.63
+VeCoR (Ours)	33.30	43.52	5.71	0.54	0.63
SiT-L/2 [28]	24.06	63.34	8.74	0.61	0.63
$+\Delta FM$ [41]	_	_	_	_	_
+VeCoR (Ours)	18.86	71.12	4.92	0.64	0.62
SiT-XL/2 [28]	20.01	74.15	8.45	0.63	0.63
$+\Delta FM$ [41]	16.32	78.07	5.08	0.66	0.63
+VeCoR (Ours)	15.56	80.96	4.70	0.67	0.62

Table 2. Main results on ImageNet-1K 256×256 using REPA-SiT backbones (same seed, 50 NFEs, Euler–Maruyama), demonstrating the generalization of our method.

Model	FID ↓	IS ↑	sFID ↓	Prec. ↑	Rec. ↑
REPA-SiT-B/2 [42]	27.33	61.60	11.70	0.57	0.64
+VeCoR (Ours)	20.39	69.09	5.57	0.61	0.64
REPA-SiT-XL/2 [42]	11.14	115.83	8.25	0.67	0.65
+VeCoR (Ours)	7.28	127.90	5.17	0.71	0.64

VeCoR Settings. By default, negatives are formed in *velocity space* via random channel shuffling with K=1, and we use a fixed contrastive weight $\lambda=0.05$. Variants in latent/image space and other operations are in Sec. 5.3.

Metrics. For class-conditional experiments, we report five standard metrics computed on 50,000 generated samples: Fréchet Inception Distance (FID) [16], Inception Score (IS) [37], spatial FID (sFID) [30], Precision (Prec.), and Recall (Rec.) [21]. For T2I, we report FID over the entire validation set. Unless otherwise specified, we use the SDE Euler–Maruyama sampler with $w_t = \sigma_t$ and set the number of function evaluations (NFE) to 50.

5.2. Main Results

Class-Conditional on ImageNet-1K Table 1 reports ImageNet-1K results with SiT backbones (S/B/L/XL). Compared to SiT baselines, VeCoR *consistently* improves nearly all metrics—especially for smaller models (FID \downarrow 14–22%, sFID \downarrow 44–53%), while recall is largely preserved and only slightly reduced at L/2 and XL/2. This suggests that explicitly constraining off-manifold directions helps the model estimate more accurate velocities and recover finer spatial details. Against the contrastive baseline Δ FM [41],

Table 3. Quantitative comparison on text-to-image generation (MS-COCO). We reproduce the result of MMDiT+REPA and do not use classifer-free guidance. RCR is denoted as Random Crop and Resize and RCS is denoted as Random Channel Shuffle.

Method	FID ↓
MMDiT+REPA [42] (SDE; NFE=50)	9.87
+VeCoR Velocity RCR (SDE; NFE=50)	7.95
+VeCoR Velocity RCS (SDE; NFE=50)	6.65

VeCoR is on par at B/2 and clearly stronger at XL/2 (lower FID/sFID with higher IS), indicating that the regularization benefits scale with model capacity.

Train with REPA Table 2 reports results with REPA-SiT backbones under a fixed 50-NFE budget at 256×256 . Relative to the REPA-SiT baselines, VeCoR reduces FID by 25-35% ($27.33\rightarrow 20.39$ on B/2; $11.14\rightarrow 7.28$ on XL/2), improves sFID by 37-52% ($11.70\rightarrow 5.57$; $8.25\rightarrow 5.17$), increases IS ($61.60\rightarrow 69.09$; $115.83\rightarrow 127.90$), and largely maintains Recall (flat at B/2 and only slightly reduced at XL/2), with small Precision gains. These results demonstrate the strong generalization ability of VeCoR across architectures and model scales.

Text-to-image on MS-COCO We evaluate VeCoR on the MS-COCO dataset using the MMDiT+REPA pipeline with a standard SDE sampler and a fixed sampling budget of NFE = 50. We reproduce the MMDiT+REPA baseline *without* classifier-free guidance [17]. Table 3 reports FID scores and compares the baseline with its VeCoRaugmented variants.

The reproduced MMDiT+REPA baseline achieves an FID of 9.87. Integrating VeCoR leads to substantial improvements under both negative-candidate constructions. Random Crop and Resize (RCR) attains an FID of 7.95, while Random Channel Shuffle (RCS) further reduces it to 6.65. These consistent gains demonstrate that velocity-contrastive regularization remains effective even without classifier-free guidance and is robust to the specific choice of negative-synthesis strategy. Overall, the results highlight VeCoR's strong generalization ability in enhancing text-to-image generation on MS-COCO.

Qualitative Results Qualitative comparisons between REPA-SiT-XL/2 and REPA-SiT-XL/2+VeCoR on ImageNet are presented in Fig. 4, while additional text-to-image results are provided in the supplementary material.

5.3. Ablation Study

Ablation Study on Negative Velocity Candidate Set As presented in Table 4, several perturbation-based variants outperform the baseline SiT-S/2 (FID = 64.26), indicating that introducing structured perturbations across different representational domains can enhance generative qual-

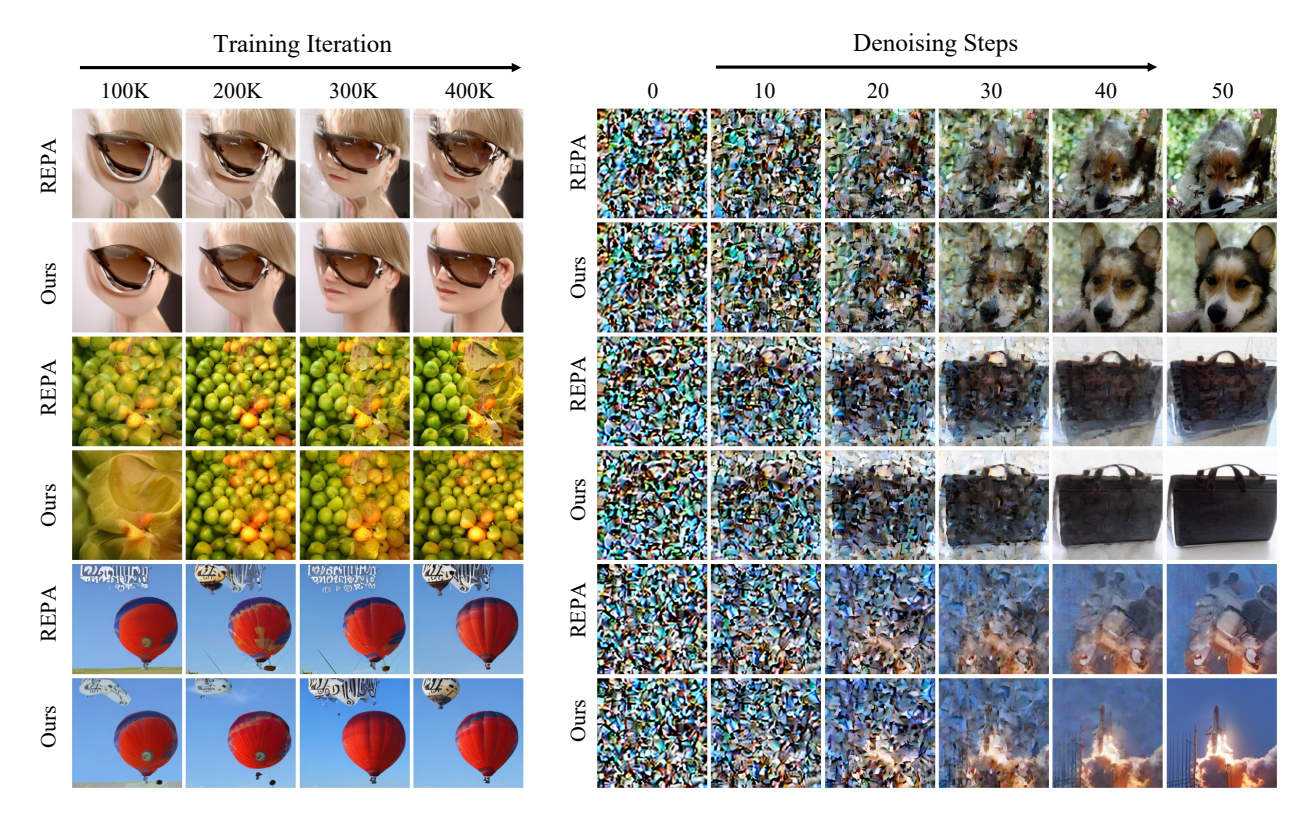


Figure 4. Qualitative comparison between REPA and our REPA-based method (VeCoR) in terms of training convergence and denoising efficiency. We compare the images generated by two SiT-XL/2 + REPA models during the first 400K iterations, one of which integrates our method, VeCoR. Both models share the same noise, sampler, and number of sampling steps, and neither uses classifier-free guidance. The left panel shows results at different training iterations. While REPA demonstrates effectiveness in accelerating convergence, our VeCoR further improves the convergence speed. The right panel illustrates the denoising process, showing that our method not only enhances training convergence but also enables the model to predict more reliable velocity fields and reconstruct the data manifold more accurately under low-step settings.

ity. When grouped by augmentation type, spatial/geometric transformations (e.g., random cropping, channel shuffling, and CutMix) generally achieve lower FID scores than appearance transformations (e.g., color jitter, Gaussian blur, and noise), particularly in the velocity space. This trend suggests that geometric perturbations, which primarily modify structural composition while preserving semantic integrity, generate more informative and dynamically consistent negative candidates. In contrast, appearance-based perturbations often introduce shallow visual variations that provide weaker supervision signals. Overall, these results highlight the advantage of modeling structural variability in the velocity domain to improve contrastive alignment and synthesis fidelity.

Ablation on Perturbation Scale and Combination We study how the perturbation scale K and operator choice shape velocity-space negatives by sweeping K and comparing geometric variants. As shown in Table 5, *Channel Shuffle* with a moderate scale (K=2) achieves the best overall trade-off, delivering the lowest FID (52.60) and sFID (6.89)

together with the highest IS (26.21) and precision (0.420). Increasing K from 2 to 3 or 4 yields only marginal changes in FID/sFID but steadily improves recall (peaking at 0.599 for $K{=}4$), suggesting diminishing returns in fidelity beyond $K{=}2$ while modestly enhancing coverage. At the small scale $K{=}1$, Channel Shuffle underperforms its $K{=}2$ counterpart, indicating insufficient diversity. Random Crop shows little sensitivity to K and consistently lags behind channel-level reconfiguration (FID $\approx 59.3{-}59.4$). Combining operators (Shuffle + Crop, $K{=}2$) increases diversity but introduces redundant variations, failing to surpass Channel Shuffle alone.

Ablation on the effect of λ . The effect of the regularization coefficient λ is illustrated in Fig. 5. When λ is too small (e.g., 0.01), VeCoR slightly improves both FID and sFID compared to SiT, but the generated images still exhibit noticeable artifacts. A moderate value (around 0.05) achieves the best trade-off, yielding lower FID and sFID scores and producing visually sharper and more natural results. However, as λ increases further (0.1–0.2), excessive regulariza-

Table 4. **FID comparison under different perturbation spaces** (columns) and augmentation types (rows). Baseline FID (64.26) of SiT-S/2 is shown for reference. Lower is better.

Perturbation Type / Operation	Image	Latent	Velocity				
<i>Baseline (SiT-S/2):</i> FID = 64.26							
Spatial / Geometric Transforma	tions						
Random Channel Shuffle	62.4	60.77	55.13				
Random Crop & Resize	62.87	62.79	59.43				
CutMix	61.94	62.98	59.62				
Appearance Transformations							
Gaussian Blur	64.18	62.28	58.73				
Gaussian Noise	63.39	64.22	65.07				
Color Jitter	63.63	65.18	64.69				

Table 5. Ablation on perturbation scale and combination. We vary the candidate size K and test geometric perturbations. Channel Shuffle with K=2 minimizes FID/sFID and maximizes IS/precision; larger K offers small recall gains without further fidelity benefits. Random Crop remains inferior and largely insensitive to K, and the combined setup (Shuffle + Crop, K=2) does not outperform Channel Shuffle alone.

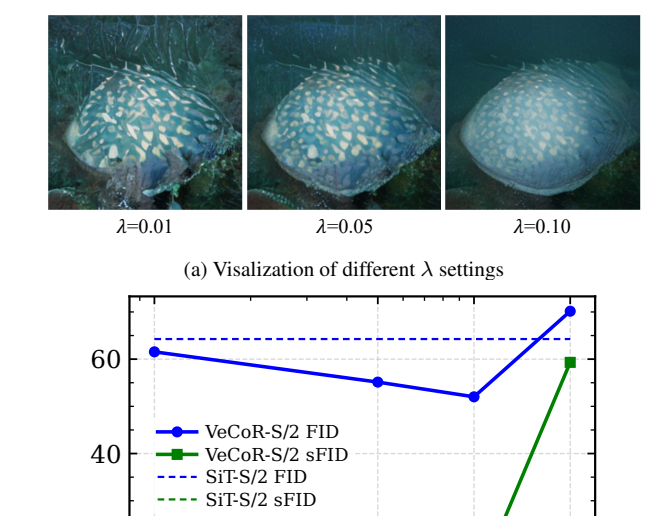
Method	FID ↓	IS ↑	sFID ↓	Precision ↑	Recall ↑
Velocity (Random Crop, $K=1$)	59.43	24.58	9.69	0.415	0.580
Velocity (Random Crop, $K=2$)	59.34	24.48	9.65	0.415	0.579
Velocity (Channel Shuffle, $K=1$)	55.13	25.48	7.406	0.416	0.592
Velocity (Channel Shuffle, $K=2$)	52.60	26.21	6.89	0.420	0.596
Velocity (Channel Shuffle, $K=3$)	53.96	25.47	7.00	0.416	0.596
Velocity (Channel Shuffle, $K=4$)	53.70	25.83	6.99	0.415	0.599
Velocity (Shuffle + Crop, $K=2$)	56.16	25.59	7.41	0.415	0.591

tion constrains the model's generative capacity, leading to the loss of fine-grained details.

Training Dynamics and Sampling Efficiency Fig. 6 compares SiT-XL/2 and SiT-XL/2+VeCoR under training and sampling budgets. In (a), FID decreases steadily with epochs for both models, but SiT-XL/2+VeCoR converges faster and attains a lower FID, indicating more effective optimization. In (b), FID drops sharply as NFE increases up to ~50 and then saturates; SiT-XL/2+VeCoR achieves lower FID in the low-NFE settings while remaining competitive at higher NFE. Together, these trends suggest that SiT-XL/2+VeCoR offers better sample efficiency and faster convergence without sacrificing asymptotic quality.

6. Conclusion

We presented **Velocity Contrastive Regularization** (**VeCoR**), a lightweight and general training scheme that extends flow matching beyond one-sided supervision, without any additional networks or external data. By coupling attraction toward reliable velocity directions with contrastive repulsion from dynamically inconsistent ones, VeCoR provides balanced, two-sided guidance that stabilizes learning and accelerates convergence. Across ImageNet and MS-COCO benchmarks, VeCoR improves



(b) Qualitative analysis of the effect of regularization coefficient λ .

0.05

λ

0.10

0.20

20

0.01

Figure 5. Ablation on the regularization coefficient λ . Comparison illustrating that a moderate λ (=0.05) yields the most natural and detailed images, while smaller or larger values cause artifacts or over-smoothed geometry.

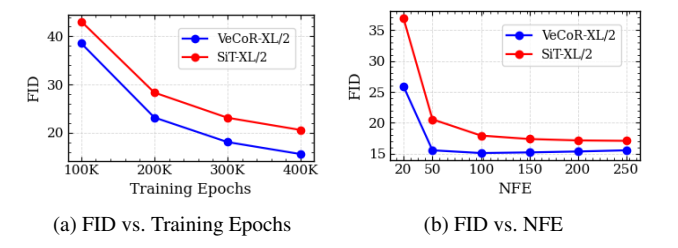


Figure 6. Training dynamics and sampling efficiency. (a) FID vs. epochs: both models improve, but SiT-XL/2+VeCoR (blue) converges faster to a lower FID than SiT-XL/2 (red). (b) FID vs. function evaluations (NFE): values drop sharply up to ~ 50 NFE then saturate; SiT-XL/2+VeCoR attains lower FID at small NFE and remains comparable at larger NFE.

fidelity and robustness, sharper structures, and faster training under the same computational budget. While the current negative sampling strategy remains heuristic and data-agnostic, future work will explore adaptive hard-negative mining and trajectory-aware perturbations to strengthen stability and efficiency further. Overall, VeCoR offers a straightforward, plug-and-play approach to more stable, data-efficient, and unified schemes for continuous generative modeling.

References

- [1] Michael S. Albergo and Eric Vanden-Eijnden. Building normalizing flows with stochastic interpolants, 2023. 5
- [2] Michael S. Albergo, Nicholas M. Boffi, and Eric Vanden-Eijnden. Stochastic interpolants: A unifying framework for flows and diffusions, 2025. 3
- [3] Philip Bachman, R Devon Hjelm, and William Buchwalter. Learning representations by maximizing mutual information across views. Advances in neural information processing systems, 32, 2019. 5
- [4] Fan Bao, Shen Nie, Kaiwen Xue, Yue Cao, Chongxuan Li, Hang Su, and Jun Zhu. All are worth words: A vit backbone for diffusion models. In *Proceedings of the IEEE/CVF con*ference on computer vision and pattern recognition, pages 22669–22679, 2023. 5
- [5] Jean-David Benamou and Yann Brenier. A computational fluid mechanics solution to the monge-kantorovich mass transfer problem. *Numerische Mathematik*, 84(3):375–393, 2000.
- [6] Ricky T. Q. Chen, Yulia Rubanova, Jesse Bettencourt, and David K Duvenaud. Neural ordinary differential equations. In Advances in Neural Information Processing Systems. Curran Associates, Inc., 2018.
- [7] Ricky T. Q. Chen, Yulia Rubanova, Jesse Bettencourt, and David Duvenaud. Neural ordinary differential equations, 2019. 1
- [8] Ting Chen, Simon Kornblith, Mohammad Norouzi, and Geoffrey Hinton. A simple framework for contrastive learning of visual representations, 2020. 5
- [9] Jia Deng, Wei Dong, Richard Socher, Li-Jia Li, Kai Li, and Li Fei-Fei. Imagenet: A large-scale hierarchical image database. In 2009 IEEE conference on computer vision and pattern recognition, pages 248–255. Ieee, 2009. 5
- [10] Prafulla Dhariwal and Alexander Nichol. Diffusion models beat gans on image synthesis. Advances in neural information processing systems, 34:8780–8794, 2021. 5
- [11] Patrick Esser, Sumith Kulal, Andreas Blattmann, Rahim Entezari, Jonas Müller, Harry Saini, Yam Levi, Dominik Lorenz, Axel Sauer, Frederic Boesel, et al. Scaling rectified flow transformers for high-resolution image synthesis. In Forty-first international conference on machine learning, 2024. 5
- [12] Weilun Feng, Chuanguang Yang, Zhulin An, Libo Huang, Boyu Diao, Fei Wang, and Yongjun Xu. Relational diffusion distillation for efficient image generation, 2024. 2
- [13] Alessio Figalli and Federico Glaudo. An invitation to optimal transport, Wasserstein distances, and gradient flows. 2021.
- [14] Will Grathwohl, Ricky T. Q. Chen, Jesse Bettencourt, Ilya Sutskever, and David Duvenaud. Ffjord: Free-form continuous dynamics for scalable reversible generative models, 2018. 1, 2
- [15] Olivier Henaff. Data-efficient image recognition with contrastive predictive coding. In *International conference on machine learning*, pages 4182–4192. PMLR, 2020. 5
- [16] Martin Heusel, Hubert Ramsauer, Thomas Unterthiner, Bernhard Nessler, and Sepp Hochreiter. Gans trained by a

- two time-scale update rule converge to a local nash equilibrium. Advances in neural information processing systems, 30, 2017. 6
- [17] Jonathan Ho and Tim Salimans. Classifier-free diffusion guidance, 2022. 6
- [18] Jonathan Ho, Ajay Jain, and Pieter Abbeel. Denoising diffusion probabilistic models. *Advances in neural information processing systems*, 33:6840–6851, 2020. 2
- [19] Tero Karras, Miika Aittala, Timo Aila, and Samuli Laine. Elucidating the design space of diffusion-based generative models. Advances in neural information processing systems, 35:26565–26577, 2022. 1
- [20] Alex Krizhevsky, Geoffrey Hinton, et al. Learning multiple layers of features from tiny images. (2009), 2009.
- [21] Tuomas Kynkäänniemi, Tero Karras, Samuli Laine, Jaakko Lehtinen, and Timo Aila. Improved precision and recall metric for assessing generative models. *Advances in neural information processing systems*, 32, 2019. 6
- [22] Sangyun Lee, Zinan Lin, and Giulia Fanti. Improving the training of rectified flows. *Advances in neural information processing systems*, 37:63082–63109, 2024. 1, 3
- [23] Tsung-Yi Lin, Michael Maire, Serge Belongie, James Hays, Pietro Perona, Deva Ramanan, Piotr Dollár, and C Lawrence Zitnick. Microsoft coco: Common objects in context. In European conference on computer vision, pages 740–755. Springer, 2014. 5
- [24] Yaron Lipman, Ricky TQ Chen, Heli Ben-Hamu, Maximilian Nickel, and Matt Le. Flow matching for generative modeling. *arXiv preprint arXiv:2210.02747*, 2022. 1, 2
- [25] Xingchao Liu, Chengyue Gong, and Qiang Liu. Flow straight and fast: Learning to generate and transfer data with rectified flow. arXiv:2209.03003, 2022. 1, 2, 3
- [26] Cheng Lu, Yuhao Zhou, Fan Bao, Jianfei Chen, Chongxuan Li, and Jun Zhu. Dpm-solver: A fast ode solver for diffusion probabilistic model sampling in around 10 steps. Advances in neural information processing systems, 35:5775– 5787, 2022. 2
- [27] Cheng Lu, Yuhao Zhou, Fan Bao, Jianfei Chen, Chongxuan Li, and Jun Zhu. Dpm-solver++: Fast solver for guided sampling of diffusion probabilistic models. *Machine Intelligence Research*, pages 1–22, 2025. 2
- [28] Nanye Ma, Mark Goldstein, Michael S. Albergo, Nicholas M. Boffi, Eric Vanden-Eijnden, and Saining Xie. Sit: Exploring flow and diffusion-based generative models with scalable interpolant transformers, 2024. 3, 6, 2
- [29] Chenlin Meng, Robin Rombach, Ruiqi Gao, Diederik P. Kingma, Stefano Ermon, Jonathan Ho, and Tim Salimans. On distillation of guided diffusion models, 2023. 2
- [30] Charlie Nash, Jacob Menick, Sander Dieleman, and Peter W Battaglia. Generating images with sparse representations. arXiv preprint arXiv:2103.03841, 2021. 6
- [31] Maxime Oquab, Timothée Darcet, Théo Moutakanni, Huy Vo, Marc Szafraniec, Vasil Khalidov, Pierre Fernandez, Daniel Haziza, Francisco Massa, Alaaeldin El-Nouby, et al. Dinov2: Learning robust visual features without supervision. arXiv preprint arXiv:2304.07193, 2023. 5

- [32] Gabriel Peyré, Marco Cuturi, et al. Computational optimal transport: With applications to data science. *Foundations and Trends® in Machine Learning*, 11(5-6):355–607, 2019. 1, 2
- [33] Alec Radford, Jong Wook Kim, Chris Hallacy, Aditya Ramesh, Gabriel Goh, Sandhini Agarwal, Girish Sastry, Amanda Askell, Pamela Mishkin, Jack Clark, et al. Learning transferable visual models from natural language supervision. In *International conference on machine learning*, pages 8748–8763. PmLR, 2021. 5
- [34] Robin Rombach, Andreas Blattmann, Dominik Lorenz, Patrick Esser, and Björn Ommer. High-resolution image synthesis with latent diffusion models. In *Proceedings of the IEEE/CVF conference on computer vision and pattern recognition*, pages 10684–10695, 2022. 5
- [35] Robin Rombach, Andreas Blattmann, Dominik Lorenz, Patrick Esser, and Björn Ommer. High-resolution image synthesis with latent diffusion models, 2022. 3
- [36] Tim Salimans and Jonathan Ho. Progressive distillation for fast sampling of diffusion models. *arXiv preprint arXiv:2202.00512*, 2022. 1, 2
- [37] Tim Salimans, Ian Goodfellow, Wojciech Zaremba, Vicki Cheung, Alec Radford, and Xi Chen. Improved techniques for training gans. *Advances in neural information processing systems*, 29, 2016. 6
- [38] Kim Shin Seong, Mingi Kwon, Jaeseok Jeong, and Youngjung Uh. Balanced conic rectified flow, 2025. 1, 3
- [39] Jiaming Song, Chenlin Meng, and Stefano Ermon. Denoising diffusion implicit models. arXiv preprint arXiv:2010.02502, 2020. 2
- [40] Yang Song, Jascha Sohl-Dickstein, Diederik P. Kingma, Abhishek Kumar, Stefano Ermon, and Ben Poole. Score-based generative modeling through stochastic differential equations, 2021. 1, 2, 3
- [41] George Stoica, Vivek Ramanujan, Xiang Fan, Ali Farhadi, Ranjay Krishna, and Judy Hoffman. Contrastive flow matching. *arXiv preprint arXiv:2506.05350*, 2025. 3, 6, 2
- [42] Sihyun Yu, Sangkyung Kwak, Huiwon Jang, Jongheon Jeong, Jonathan Huang, Jinwoo Shin, and Saining Xie. Representation alignment for generation: Training diffusion transformers is easier than you think. *arXiv preprint arXiv:2410.06940*, 2024. 5, 6
- [43] Sangdoo Yun, Dongyoon Han, Seong Joon Oh, Sanghyuk Chun, Junsuk Choe, and Youngjoon Yoo. Cutmix: Regularization strategy to train strong classifiers with localizable features, 2019. 5
- [44] Kaiwen Zheng, Cheng Lu, Jianfei Chen, and Jun Zhu. Dpm-solver-v3: Improved diffusion ode solver with empirical model statistics. Advances in Neural Information Processing Systems, 36:55502–55542, 2023. 2
- [45] Zhenyu Zhou, Defang Chen, Can Wang, Chun Chen, and Siwei Lyu. Simple and fast distillation of diffusion models, 2024. 1, 2

VeCoR — **Velocity Contrastive Regularization for Flow Matching**

Supplementary Material

A. More Implementation Details

This section elucidates more details about the concrete augmentation-like perturbation in Sec. 4.2.

A.1. Augmentation-like Perturbation Details

Given a batch input $z_+ \in \mathbb{R}^{B \times C \times H \times W}$, which may represent training images (\hat{I}_+) , latents (\hat{x}_+) , or velocities (\hat{v}_+) , our goal is to apply augmentation-like perturbations to obtain negative samples z_- .

Random Channel Shuffle We apply a per-sample cyclic channel shift to ensure that no channel remains in its original position. Given $z_+ \in \mathbb{R}^{B \times C \times H \times W}$, a shift $k \in \{1,\ldots,C-1\}$ is sampled and applied via modular indexing, producing the perturbed output z_- .

Random Crop and Resize For a batch input $z_+ \in \mathbb{R}^{B \times C \times H \times W}$, we uniformly sample the target area ratio and aspect ratio:

$$\alpha \sim \mathcal{U}(\text{scale}_{\min}, \text{scale}_{\max}), \qquad r \sim \mathcal{U}(\text{ar}_{\min}, \text{ar}_{\max}),$$

with default $\alpha \in [0.9, 0.95]$ and $r \in [0.95, 1.05]$. The target crop area is

$$A_{\rm crop} = \alpha(HW),$$

and the crop dimensions are

$$h = \sqrt{\frac{A_{
m crop}}{r}}, \qquad w = \sqrt{A_{
m crop}\,r},$$

rounded to integers and clamped to valid ranges. If the sampled dimensions fall below a threshold, we fall back to a larger crop (e.g., $0.9H \times 0.9W$). A valid crop location is sampled uniformly, and the cropped region is resized back to (H,W), resulting in z_- .

CutMix Given a batch $z_+ \in \mathbb{R}^{B \times C \times H \times W}$, we first construct a derangement permutation

$$\pi: \{1, \dots, B\} \to \{1, \dots, B\}$$

that satisfies $\pi(i) \neq i$ for every index i, ensuring that no sample is mixed with itself.

For each sample $z_{+}^{(i)}$, we draw a mixing coefficient

$$\lambda^{(i)} \sim \text{Beta}(\alpha, \alpha), \qquad \alpha = 1.$$

and compute the CutMix region scale

$$r^{(i)} = \sqrt{1 - \lambda^{(i)}}.$$

The corresponding box width and height are

$$w^{(i)} = r^{(i)}W$$
, $h^{(i)} = r^{(i)}H$.

A box center (c_x, c_y) is sampled uniformly over the spatial domain. The bounding coordinates are then clipped to valid image ranges:

$$x_{1} = \operatorname{clip}\left(c_{x} - \frac{w^{(i)}}{2}, 0, W\right),$$

$$x_{2} = \operatorname{clip}\left(c_{x} + \frac{w^{(i)}}{2}, 0, W\right),$$

$$y_{1} = \operatorname{clip}\left(c_{y} - \frac{h^{(i)}}{2}, 0, H\right),$$

$$y_{2} = \operatorname{clip}\left(c_{y} + \frac{h^{(i)}}{2}, 0, H\right).$$

Finally, the rectangular region of $z_+^{(i)}$ within $(x_1:x_2,y_1:y_2)$ is replaced by the corresponding patch from the paired sample $z_+^{(\pi(i))}$, yielding the CutMix-perturbed output $z_+^{(i)}$.

Gaussian Blur Given a batch input $z_+ \in \mathbb{R}^{B \times C \times H \times W}$, we apply a per-channel Gaussian blur with kernel size k (odd) and standard deviation $\sigma \geq 1$. We use k=5 and $\sigma=1$.

The kernel is

$$G(u, v) = \exp\left(-\frac{u^2 + v^2}{2\sigma^2}\right), \quad u, v \in \left[-\frac{k-1}{2}, \frac{k-1}{2}\right],$$

normalized so that $\sum_{u,v} G(u,v) = 1$.

We replicate the kernel across channels:

$$K \in \mathbb{R}^{C \times 1 \times k \times k}, \qquad K_c = G,$$

and apply depthwise convolution with reflection padding

$$p = \left| \frac{k}{2} \right|,$$

which prevents artificial dark borders or edge artifacts that would otherwise arise from zero-padding during Gaussian smoothing. Finally, the blurred output defines z_{-} .

Gaussian Noise Given a batch input $z_+ \in \mathbb{R}^{B \times C \times H \times W}$, we compute a noise scale for each individual sample $z_+^{(i)} \in \mathbb{R}^{C \times H \times W}$

For each sample, we first measure its per-sample standard deviation:

$$\sigma^{(i)} = \operatorname{std}\left(z_{+}^{(i)}\right), \qquad \tilde{\sigma}^{(i)} = \frac{\sigma^{(i)}}{\sigma_{\max}},$$

where σ_{max} is the maximum standard deviation observed within the batch.

We then define the noise magnitude as

$$\gamma^{(i)} = \text{base_scale} (1 - \tilde{\sigma}^{(i)}),$$

where base_scale is set to 255 in image space and to 1 in both latent and velocity spaces.

Finally, we inject Gaussian noise into each sample to get $z^{(i)}$:

$$z_{-}^{(i)} = z_{+}^{(i)} + \gamma^{(i)} \, \varepsilon^{(i)}, \qquad \varepsilon^{(i)} \sim \mathcal{N}(0, 1).$$

Color Jitter Given a batch $z_+ \in \mathbb{R}^{B \times C \times H \times W}$, we apply per-sample color jitter composed of brightness, contrast, and saturation adjustments. We first normalize the input to obtain z', and independently sample the jitter factors from

$$\lambda_{\rm b}, \lambda_{\rm c}, \lambda_{\rm s} \sim \mathcal{U}(1-\delta, 1+\delta), \qquad \delta = 0.2.$$

Brightness.

$$z' \leftarrow \lambda_{\rm b} z_+$$
.

Contrast. Let $\mu = \text{mean}(z')$ denote the global mean intensity:

$$z' \leftarrow (z' - \mu)\lambda_c + \mu$$
.

Saturation. Let $g = \text{mean}_c(z')$ be the per-pixel channel average:

$$z' \leftarrow (z' - q)\lambda_s + q$$
.

These three operators are applied in a random order. The final result is clamped to [0,1] and rescaled as needed to obtain z_- .

B. More Results

In this section, we provide additional quantitative and qualitative results.

B.1. ImageNet-1K Results with ODE Sampling

Tab. 6 reports the ImageNet-1K results under ODE sampling. Across all SiT backbones, integrating VeCoR yields clear improvements in the main quality metrics, achieving lower FID and higher IS under the same sampling budget (50 NFEs, Heun2).

Table 6. Results on ImageNet-1K 256×256 using SiT backbones (same seed, 50 NFEs, Heun2).

Model	$\textbf{FID}\downarrow$	IS \uparrow	$\mathbf{sFID}\downarrow$	Prec. ↑	Rec. ↑
SiT-S/2 [28]	59.28	23.43	9.33	0.40	0.59
+VeCoR (Ours)	55.11	24.34	8.53	0.41	0.59
SiT-B/2 [28]	37.07	40.27	6.79	0.51	0.65
+VeCoR (Ours)	33.76	41.22	7.76	0.53	0.63
SiT-L/2 [28]	21.9	63.84	5.58	0.61	0.64
+VeCoR (Ours)	19.81	66.16	7.41	0.63	0.62
SiT-XL/2 [28]	18.59	72.05	5.30	0.63	0.64
+VeCoR (Ours)	16.55	76.17	7.21	0.65	0.62

Although FID, IS, and Precision improve, we observe mild decreases in sFID and Recall under certain configurations. A possible explanation is that, in a fully deterministic ODE setting, the additional signals from VeCoR about "where not to go" may guide the trajectory to remain closer to certain regions of the manifold, which could slightly limit the diversity of viable generation paths.

Overall, these shifts are small relative to the overall gains, and VeCoR remains beneficial under both SDE- and ODE-based sampling.

B.2. Text-to-Image Qualitative Results

We provide the text-to-image visual comparisons in Fig. 7, which illustrate that, under identical sampling conditions, incorporating VeCoR leads to outputs with better color consistency and stronger semantic alignment to the input prompts.

C. On the Effectiveness of the VeCoR Loss

For completeness, we provide the analytical form of our velocity contrastive regularization (VeCoR). Although its structure resembles the contrastive FM objective in Δ FM [41], the intent is fundamentally different: Δ FM leverages contrastive signals *across conditions* to enforce class-level separability, whereas our formulation applies contrastive supervision directly at the *dynamics level* to enhance trajectory stability and suppress off-manifold drift during sampling. Thus, despite superficial similarities, the contrastive role in VeCoR is intrinsically distinct.

We begin by expressing the VeCoR objective in its expectation form:

$$\mathcal{L}^{(\text{VeCoR})}(\theta) = \mathbb{E}\left[\|\mathbf{v}_{\theta}(\hat{x}_{t}, t) - \hat{\mathbf{v}}_{+}\|_{2}^{2} - \lambda \sum_{k=1}^{K} \|\mathbf{v}_{\theta}(\hat{x}_{t}, t) - \hat{\mathbf{v}}_{-}^{(k)}\|_{2}^{2}\right],$$
(8)

where the expectation is taken over timesteps, perturbed states \hat{x}_t , and injected noise.

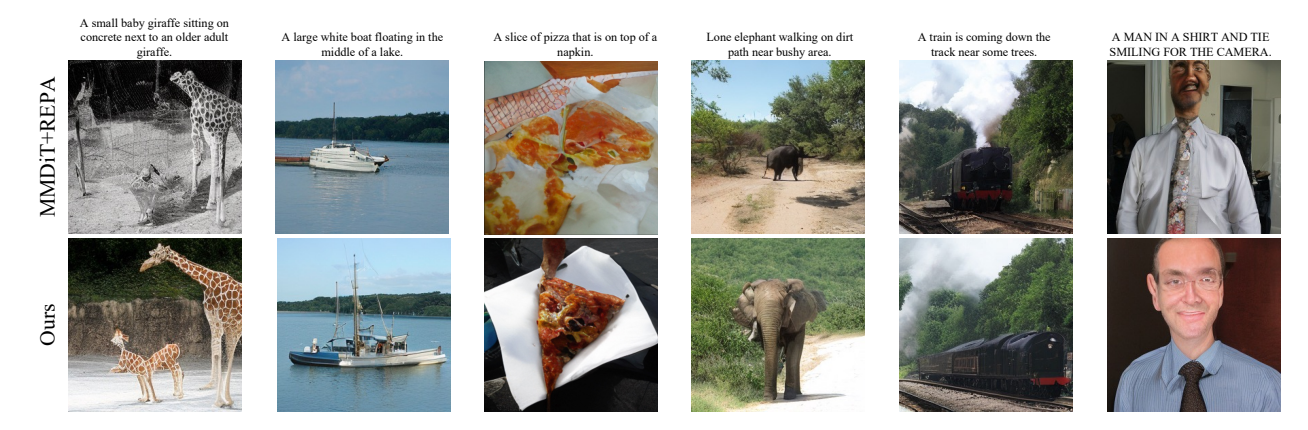


Figure 7. Qualitative comparison on text-to-image generation (MS-COCO). We use classifier-free guidance with w = 2.0 and using (same seed, 50 NFEs, Euler–Maruyama).

Step 1: Expand and collect quadratic terms. Let $\mathbf{v}_{\theta} = \mathbf{v}_{\theta}(\hat{x}_t,t)$ for brevity. Expanding the squared terms and applying linearity of expectation yields

$$\mathcal{L}^{(\text{VeCoR})}(\theta) = \mathbb{E}\Big[(1 - \lambda K) \, \mathbf{v}_{\theta}^{\top} \mathbf{v}_{\theta} \\ - 2 \, \mathbf{v}_{\theta}^{\top} \Big(\hat{\mathbf{v}}_{+} - \lambda \sum_{k=1}^{K} \hat{\mathbf{v}}_{-}^{(k)} \Big) \Big] + \text{const},$$
(9)

where the constant aggregates all terms independent of v_{θ} .

Step 2: Compute the minimizer. Taking the gradient of (9) with respect to v_{θ} and setting it to zero gives

$$2(1 - \lambda K) \mathbf{v}_{\theta}^* = 2 \mathbb{E} \left[\hat{\mathbf{v}}_+ - \lambda \sum_{k=1}^K \hat{\mathbf{v}}_-^{(k)} \right]. \tag{10}$$

Dividing both sides by $2(1-\lambda K)$ yields the closed-form solution:

$$\mathbf{v}_{\theta}^* = \frac{\mathbb{E}[\hat{\mathbf{v}}_+] - \lambda \sum_{k=1}^K \mathbb{E}[\hat{\mathbf{v}}_-^{(k)}]}{1 - \lambda K}.$$
 (11)

This derivation shows that the VeCoR objective preserves the FM fixed point while adding a contrastive correction that suppresses destabilizing dynamical alternatives. Unlike ΔFM —whose contrastive term separates flows across conditioning labels—the negative velocities in VeCoR represent dynamical directions that would drive trajectories toward undesirable, off-manifold evolution. In this view, VeCoR acts as a corrective force that steers the predicted velocity away from off-manifold directions and reinforces stable, data-consistent trajectories. To maintain this behavior in a mathematically well-posed manner, the quadratic coefficient $(1-\lambda K)$ must remain positive, ensuring that the objective retains a proper minimization structure. This leads to the requirement

$$\lambda K < 1$$
,

which prevents the loss from becoming ill-conditioned.